IEEE Access
Multidisciplinary ⋮ Rapid Review ⋮ Open Access Journal

Received September 11, 2019, accepted October 12, 2019, date of publication November 6, 2019,
date of current version November 19, 2019.

Digital Object Identifier 10.1109/ACCESS.2019.2951802

Side Lobe Suppression and Gain Retaining of Practical Space-Borne Active Phased Antenna Array With Triangular Grids

CHENG ZHANG[1], ANYONG QING[1,2], (Senior Member, IEEE), AND YIZHE ZHAO[1]
[1]School of Physics, University of Electronic Science and Technology of China, Chengdu 610054, China
[2]School of Electrical Engineering, Southwest Jiaotong University, Chengdu 611756, China

Corresponding author: Anyong Qing (qinganyong@tsinghua.org.cn)

This work was supported in part by the U.S. Department of Commerce under Grant BS123456.

ABSTRACT In a practical space-borne active phased antenna array (APAA), main beam scanning angle (MBSA)-dependent low side lobe level (SLL) and taper loss are the ultimate and most critical performances. At some MBSA, extremely SLL in some local space is needed. The harsh limitation on APAA taper loss further complicates the problem seriously. In this paper, the main beam scanning space (MBSS) was divided into several subspaces. Instead of applying a single set of weights regardless of the MBSA, a separate set of weights is implemented independently in each subspace. This transforms the nearly unsolvable problem into multiple solvable problems. An array-decomposition approach is proposed to further reduce the number of synthesis parameters for each subspace. The entire array is simplified as an assembly of multiple sub-arrays. Each and every sub-array shares the same set of weights. The number of synthesis parameters is therefore reduced to the order of the subarray that the synthesis is much easier to solve without sacrificing too much synthesis performance. The proposed approach has been applied to solve concerned practical problem successfully.

INDEX TERMS APAA, SLL, taper loss, space division, array-decomposition.

I. INTRODUCTION

In recent years, active phased antenna array (APAA) has been increasingly applied in satellites due to its advantages such as rapid beam scanning abilities, high reliability, more flexibility for different kinds of application and multi-functionality [1]. In a practical application, an APAA as shown in Fig.1 receives signals from the earth and communicates with other satellites. The array employs triangular arrangement of elements to obtain higher gain and lower element density [2].

The APAA receives signals from the earth ($0° \le \theta_0 < 20°$, $0° \le \varphi_0 \le 360°$) and communicates with other satellites ($20° \le \theta_0 \le 60°$, $0° \le \varphi_0 \le 360°$), where ($\theta_0$, φ_0) is the MBSA. It is well known that amplitude and/or phase tapering usually results in reduction of beam efficiency and power attenuation. Both will lead to gain loss which is termed taper loss here. In this paper, we focus on minimizing taper loss.

Requirements on the SLL and gain loss change as its function changes. In particular,

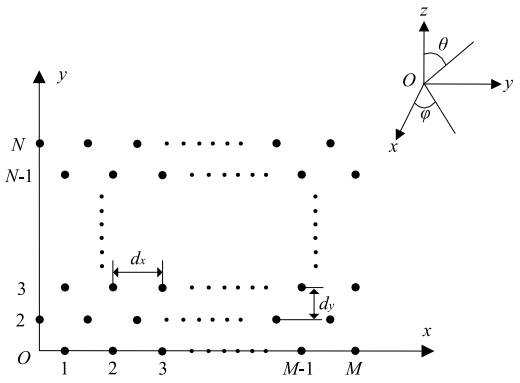

FIGURE 1. The planar array with elements spaced at triangular grids.

(a) When the APAA receives signals from the earth, the main beam scans $0° \le \theta_0 < 20°$, $0° \le \varphi_0 \le 360°$. SLL ≤ -25 dB in entire visible space $0 \le \sqrt{u^2 + v^2} \le 1$ is required to ensure high signal to noise ratio (SNR); the taper loss $\le$ 5.5 dB, and the dynamic range ratio (DRR) $<$ 15 dB;

The associate editor coordinating the review of this manuscript and approving it for publication was Yang Yang.

(b) When the APAA communicates with other satellites, the main beam scans space ($20° \leq \theta_0 \leq 60°, 0° \leq \varphi_0 \leq 360°$), SLL ≤ -30dB in the space $0 \leq \sqrt{u^2+v^2} \leq 0.2$, SLL ≤ -13 dB in the space $0.2 < \sqrt{u^2+v^2} \leq 1$; the taper loss $\leq$ 2 dB, and DRR < 15 dB.

Classic methods such as Chebyshev method [3] and Taylor method [4] are applied to suppress the side lobes in the entire visible space by amplitude-only control. However, due to over-attenuation of excitation currents especially for elements near array edge, taper loss is too large that both methods fail to produce qualified APAA. The Woodward-Lawson method [5] is also used for main beam forming. Likewise, it fails because the SLL is above the specified level.

In nature, synthesis of APAA is a multi-dimension multi-objective optimization problem. As such, in recent years, genetic algorithms (GA) [6]-[7], particle swarm optimization (PSO) algorithm [8]-[9], differential evolution [10]-[11] and other intelligent optimization algorithms have been successfully employed in antenna array pattern synthesis. However, all of them suffer the ''curse of dimensionality''.

To reduce the number of optimization variables and improve convergence speed, Li Shi proposed a method which using the weights of a set of the orthogonal basis functions as optimizing variables [12]. It may be have the ability to optimize the excitation currents of array with hundreds or thousands elements. Fig. 2 shows the synthesized patterns with different beam directions. For the pattern with broadside main beam, it has a maximum sidelobe level of -19dB; for other patterns with scanning main beams, the maximum SLL are higher than -19dB. Obviously, the result fails to meet the SLL requirements.

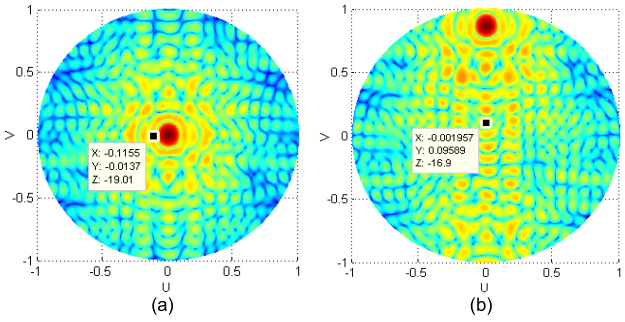

FIGURE 2. Array patterns synthesized by the Li Shi's method (a) $\theta_0 = 0°$, $\varphi_0 = 0°$, (b) $\theta_0 = 60°$, $\varphi_0 = 90°$.

The successive fast Fourier transform (SFFT) is more flexibility, and ease of implementation in software [13]. It is applied to synthesize the above mentioned APAA.

Two cases have been considered. The first one is the worst scenario synthesis in the entire MBSS. The synthesized weights apply to all MBSA. Unfortunately, the worst scenario requirements in the entire MBSS usually make the synthesis unrealistic. As a demonstration, the patterns with MBSA at $\theta_0 = 60°$, $\varphi_0 = 0°$ obtained by using amplitude- and phase-only synthesis to suppress side lobes down to SLL $= -30$ dB are depicted in Fig. 3. The former result fails

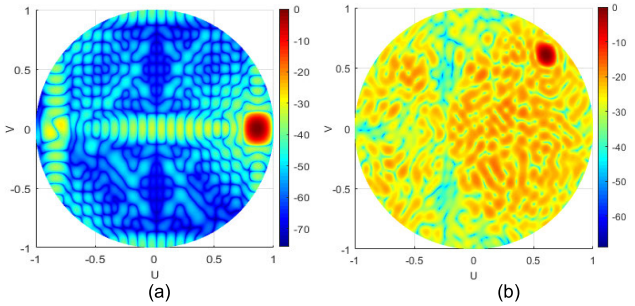

FIGURE 3. Synthesized patterns (a) Pattern synthesized by amplitude-only control, and (b) Pattern synthesized by phase-only control.

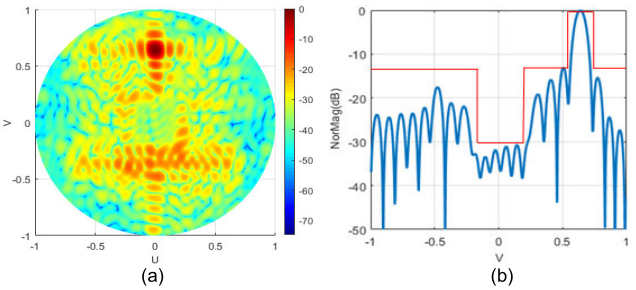

FIGURE 4. Patterns with main beam scanning at ($\theta_0 = 40°$, $\varphi_0 = 90°$). (a) 3-D pattern, and (b) v-cuts at $u = 0$.

to meet the taper loss requirements while the latter one meets neither SLL requirements nor taper loss requirements.

The above observation hints that there might be no single universal weights for the APAA to simultaneously satisfy the specific requirements on side lobe level and taper loss.

The second one is the point by point synthesis at each and every MBSA in the entire MBSS. When the main beam steers at a given direction, it is observed that this method succeeds in both side lobe suppression and taper loss. For example, as shown in Fig. 4, when the main beam steers at ($\theta_0 = 40°$, $\varphi_0 = 90°$), SLL ≤ -30 dB in the space $0 \leq \sqrt{u^2+v^2} \leq 0.2$, SLL ≤ -13 dB in the space $0.2 < \sqrt{u^2+v^2} \leq 1$, and the taper loss is 1.5 dB.

In practice, resolution of scanning angle is 0.05° or finer. Enumeration of all synthesis cases for the concerned practical application would mount to at least 1200×7200. It is apparently impractical in terms of synthesis time and flash RAM.

In this paper, a scanning space-division and array-decomposition approach is proposed to solve this hard problem. Instead of applying a single set of weights regardless of the scanning angle, different weights are implemented when the APAA is scanning at different angles. In another word, the scanning space is divided into multiple sub-spaces in which different weights are implemented. In addition, to ease the synthesis problem in each sub-space, the entire array is simplified as an assembly of multiple sub-arrays. Each and every sub-array shares the same set of scanning angle-dependent weights. The number of synthesis parameters is therefore reduced to the order of the subarray that the

synthesis is much easier to solve without sacrificing too much synthesis performance.

II. DIVISION OF MAIN BEAM SCANNING SPACE

Consider a general planar antenna array with elements arranged in a triangular grid as shown in Fig. 1. By the principle of vector superposition (PVS) [14], the array pattern can be expressed as

$$F(u_{kl}, v_{kl}) = \sum_{m=1}^{M}\sum_{n=1}^{N} I_{mn} e^{j\psi_{mn}} EF_{mn}(u_{kl}, v_{kl}) e^{j\beta(x_{mn}u_{kl}+y_{mn}v_{kl})} \tag{1}$$

where $u_{kl} = \sin\theta_k \cos\varphi_l$ and $v_{kl} = \sin\theta_k \sin\varphi_l$, $k = 0, \ldots, K-1$, $l = 0, \ldots, L-1$, I_{mn} and ψ_{mn} are the excitation current magnitude and phase of the (m, n)th element when the main beam steers at (θ_0, φ_0), $EF_{mn}(u_{kl}, v_{kl})$ is the pattern of element(m, n) which is included in Eq. (1) to highlight the practical significance of the presented study, $\beta = 2\pi/\lambda$is the phase constant, λ is the wavelength, respectively,

$$\psi_{mn} = \varphi_{mn} - \beta(x_{mn}u_0 + y_{mn}v_0) \tag{2}$$

where $u_0 = \sin\theta_0 \cos\varphi_0$, $v_0 = \sin\theta_0 \sin\varphi_0$. The first term on the right hand side of Eq. (2) is the weighting phase which is used to suppress SLL or beamforming, while the second term is used to change the main beam direction.

Without loss of generality, all elements in the array is assumed identical. Practical testing shows that

$$EF_{mn}(u_{kl}, v_{kl}) \approx EF(u_{kl}, v_{kl}) \approx \cos^p\theta_k, \quad 0 \le \theta \le \frac{\pi}{2} \tag{3}$$

where $p = 0.85$.

In this case, Eq. (1) can be re-written as

$$F(u_{kl}, v_{kl}) = EF(u_{kl}, v_{kl}) \cdot AF(u_{kl}, v_{kl}) \tag{4}$$

where

$$AF(u_{kl}, v_{kl}) = \sum_{m=1}^{M}\sum_{n=1}^{N} I_{mn} e^{j\varphi_{mn}} e^{j[\beta x_{mn}(u_{kl}-u_0)+\beta y_{mn}(v_{kl}-v_0)]} \tag{5}$$

According to the aforementioned observation, both I_{mn} and φ_{mn} are dependent on θ_0 and φ_0, i.e.,

$$I_{mn} = I_{mn}(u_0, v_0) \tag{6}$$

$$\varphi_{mn} = \varphi_{mn}(u_0, v_0) \tag{7}$$

As mentioned in Section I, point by point synthesis at each and every MBSA in the entire MBSS is impractical in terms of synthesis time and flash RAM. Empirical experience implies that both I_{mn} and φ_{mn} only weakly couple with θ_0 and φ_0. As such, in our practice, they are piecewisely approximated as

$$I_{mn}(u_0, v_0) = I^g_{mn}, \quad g = 1, 2, ..., G \tag{8}$$

$$\varphi_{mn}(u_0, v_0) = \varphi^g_{mn}, \quad g = 1, 2, ..., G \tag{9}$$

where G is the number of sub-spaces of the entire scanning space.

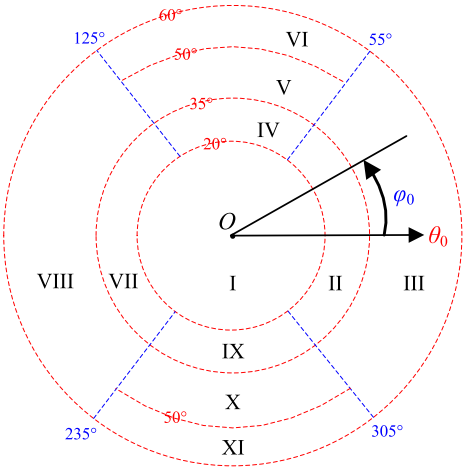

FIGURE 5. Division diagram of scanning space.

As can be seen from the specified requirements, in MBSS $0° \le \theta_0 < 20°$, $0° \le \varphi_0 \le 360°$, lower SLL is more important for better receiving signals from the earth, while the taper loss is eased to 5.5 dB. Therefore, the MBSS $0° \le \theta_0 < 20°$, $0° \le \varphi_0 \le 360°$ is treated as subspace I. Amplitude-only synthesis by using SFFT is applied.

When the APAA communicates with other satellites, the main beam scans at space ($20° \le \theta_0 \le 60°$, $0° \le \varphi_0 \le 360°$). In this case, higher gain is crucial for long distance communication between satellites due to power limitation. Therefore, phase-only synthesis is applied. In addition, to suppress clutter and/or interference from the earth, SLL ≤ -30 dB is required in the space $0 \le \sqrt{u^2+v^2} \le 0.2$. It is very unlikely to meet this harsh requirement by a single set of weighting phases for all MBSA. Therefore, this MBSS is further divided into 10 subspaces as shown in Fig. 5. In particular, it is finer in the space ($35° \le \theta_0 < 60°$, $55° \le \varphi_0 \le 125°$) and ($35° \le \theta_0 < 60°$, $235° \le \varphi_0 \le 305°$) since it is observed that the side lobes near the normal direction are more difficult to suppress when the main beam is scanning at these space. The phase synthesis approach for those subspaces is given in Section III and Section IV.

In addition, the synthesized weights are stored at the flash RAM of APAA. The APAA calls the corresponding weighting data when the main beam scans at different subspaces. Therefore, the scanning speed is not affected.

III. ARRAY DECOMPOSITION

The division of scanning space complicates a single synthesis problem into 11 synthesis problems. By making use of symmetry, there are still 6 independent synthesis problems (I, II, III, IV, V and VI). Each synthesis problem involves $2MN$ parameters (magnitudes and phases of elements). Usually, M and N are large. It is therefore more urging to reduce the dimension of synthesis problem.

According to antenna theory [15], the pattern of the rectangularly arranged array with rectangular boundary and separable distribution can be represented as the product of two patterns, one each from two orthogonal linear arrays. In this case,

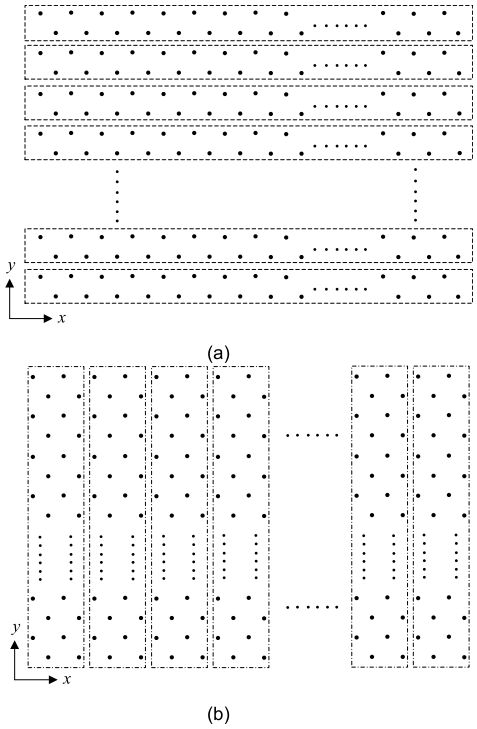

FIGURE 6. Array decomposed by two approaches (a) array decomposed by every two rows of elements, (b) array decomposed by every two columns of elements.

the synthesis problem of such planar arrays can be simplified as two independent synthesis problems of linear arrays. Hence the number of optimization parameters is significantly reduced from $2MN$ to $2M + 2N$ that the computational cost is affordable and usually the synthesized antenna arrays are practically acceptable.

Inspired by the above findings, in this paper, the triangularly arranged planar array with rectangular boundary is assumed one with separable distribution and is treated as an equivalent rectangularly arranged array with rectangular boundary and separable distribution.

Decomposition of the entire antenna array can be carried out in two ways. The first approach regards every two rows of elements as a subarray as shown in Fig. 6(a), and the second approach combines every two columns of elements as a subarray as shown in Fig. 6(b).

The former decomposition is implemented to synthesize the element excitations when the main beam scans at the II∼III, Eq. (5) can be re-written as

$$AF(u_{kl}, v_{kl}) = AF_{subarray\_R}(u_{kl}, v_{kl}) \cdot \sum_{n=1}^{N/2} I_n e^{j\psi_n} e^{j2\beta n d_y v_{kl}} \tag{10}$$

where

$$AF_{subarray\_R}(u_{kl}, v_{kl}) = \sum_{m=1}^{M} \sum_{n=1}^{2} I_{mn}^{g} e^{j\varphi_{mn}^{g}} e^{j\beta[x_{mn}(u_{kl}-u_0)+y_{mn}v_{kl}]} \tag{11}$$

$g = 1, 2$, and $u_0 = \sin\theta_0$.

The latter decomposition is taken to synthesize the element excitations when the main beam scans at the IV∼ VI, Eq. (5) can be re-written as

$$AF\ (u_{kl}, v_{kl}) = AF_{subarray\_C}\ (u_{kl}, v_{kl}) \cdot \sum_{m=1}^{M/2} I_m e^{j\psi_m} e^{j2\beta m d_x u_{kl}} \tag{12}$$

where

$$AF_{subarray\_C}\ (u_{kl}, v_{kl}) = \sum_{m=1}^{2} \sum_{n=1}^{N} I_{mn}^{g} e^{j\varphi_{mn}^{g}} e^{j\beta[x_{mn}u_{kl}+y_{mn}(v_{kl}-v_0)]} \tag{13}$$

$g = 4, 5, 6$, and $v_0 = \sin\theta_0$.

With the aim of lower taper loss of the array, the phase only control is used, thus in Eqs. (11) and (13), $I_{mn}^{g} = 1$, $I_m = 1$ and $I_n = 1$. According to the need of optimization, $\psi_m = 0$ and $\psi_n = 0$ in Eqs. (10) and (12), respectively.

Obviously, the dimension of synthesis problem is significantly reduced from $O(M \times N)$ to only $O(2N)$ or $O(2M)$. In addition, it can be further noticed that the computational efficiency of array pattern is also greatly improved.

IV. OPTIMIZATION OF WEIGHTING PHASE

As a powerful stochastic global optimization algorithm, dynamic differential evolution (DDE) [16] is applied to optimize the phase values of subarray elements. In view of the APAA requirements and the proposed scanning space-division and array-decomposition approach, the fitness function for subspace g can be expressed as

$$\begin{aligned} &objf_g \\ &= \omega_{1g} \times \max[20 \times \log_{10} \frac{\underset{(u_{kl},v_{kl})\in S1_g}{\left|F_g(u_{kl}, v_{kl})\right|}}{\max(\underset{(u_{kl},v_{kl})\in S}{\left|F_g(u_{kl}, v_{kl})\right|})} - C1_g, 0]^2 \\ &\quad + \omega_{2g} \times \max[20 \times \log_{10} \frac{\underset{(u_{kl},v_{kl})\in S2_g}{\left|F_g(u_{kl}, v_{kl})\right|}}{\max(\underset{(u_{kl},v_{kl})\in S}{\left|F_g(u_{kl}, v_{kl})\right|})} - C2_g, 0]^2 \\ &\quad + \omega_{3g} \times (D_{0g} - D_g) \end{aligned} \tag{14}$$

where ω_{1g}, ω_{2g} and ω_{3g} are weight coefficients controlling the sensitivity of the optimization procedure, $C1_g$ and $C2_g$ are negative numbers which are smaller than -30 and -13, respectively. D_{0g} is the directivity of the APAA with uniform amplitudes and no weighting phase, D_g is the directivity of the APAA with uniform amplitudes and weighing phases. S_g, $S1_g$ and $S2_g$ are three regions which can be given by

$$S = [(u_{kl}, v_{kl}) \in \text{the entire visible space}] \tag{15}$$

$$S1_g = (u_{kl}, v_{kl} \left| 0 \le \sqrt{u_{kl}^2 + v_{kl}^2} \le \beta_g \right.) \tag{16}$$

$$S2_g = (u_{kl}, v_{kl} \left| \beta_g < \sqrt{u_{kl}^2 + v_{kl}^2} \le 1 \right.) \text{ and } (u_{kl}, v_{kl}) \notin S3_g) \tag{17}$$

TABLE 1. The value of parameters in this application.

subspace	ω_1	ω_2	ω_3	C_1	C_2	β	θ_0	φ_0	D_0
II	2	1.4	2.5	-31	-13.5	0.33	27.5°	0°	31.6
III	1	1	4	-31	-13.5	0.42	47.5°	0°	29.6
IV	2	1.4	3	-31	-14	0.33	27.5°	90°	31.6
V	1	1	4	-32	-14	0.35	42.5°	90°	30.2
VI	2	1	3	-32	-14	0.27	55°	90°	28.4

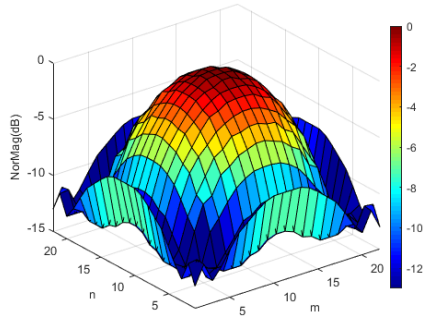

FIGURE 7. The Weighting Amplitude Distribution.

TABLE 2. Psll in Subspace I.

θ_0	φ_0	PSLL (dB)
0°	0°	-26
19.9°	0°	-25.3
19.9°	45°	-25.4
19.9°	90°	-25.3

and

$$S3_g = [(u_{kl}, v_{kl}) \in \text{the main lobe region}] \qquad (18)$$

where β_g is a positive number between 0.2 and 1.

The above mentioned parameters are shown in TABLE 1.

V. NUMERICAL RESULTS

The concerned array has $N = 22$ rows of elements and the vertical distance between two adjacent rows is $d_y = 0.5\lambda$. Each row has $M = 22$ equally spaced elements and the horizontal spacing between two adjacent elements in a row is $d_x = 0.59\lambda$.

Subspace I

The weighting magnitude synthesized by using the SFFT is plotted in Fig. 7. The dynamic range ratio (DRR) is 13 dB which is lower than the specified 15 dB. The directivity of this concerned array at broadside is 32.5 dBi and 31.6 dBi with uniform excitations and the weighting magnitudes, respectively. The gain loss is 0.9 dB and power loss is 4.5 dB. Accordingly, the taper loss is 5.4 dB, less than the required 5.5 dB.

The peak SLL (PSLL) values when the main beam scans at representative directions are summarized in TABLE 2. Obviously, PSLL meets the requirements.

To have a more straightforward illustration of the SLL, the radiation pattern with main beam scans at $\theta_0 = 19.9°$, $\varphi_0 = 45°$ is given in Fig. 8.

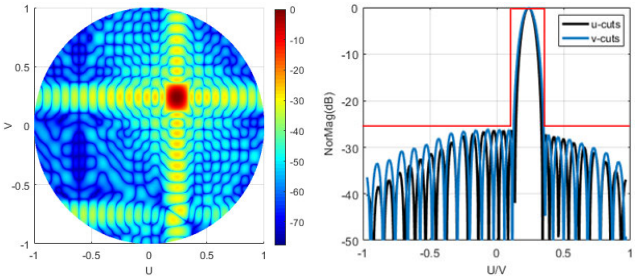

FIGURE 8. Patterns with main beam scanning at ($\theta_0 = 19.9°$, $\varphi_0 = 45°$). (a) 3-D pattern, and (b) *u*-cuts and *v*-cuts.

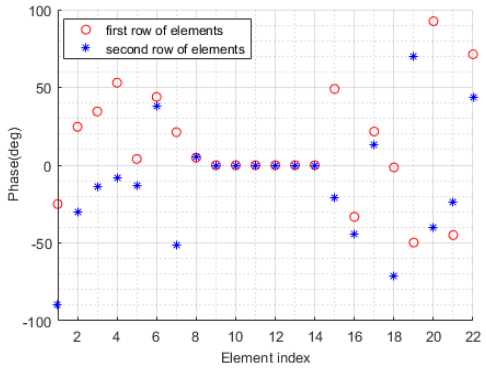

FIGURE 9. Weighting phases.

TABLE 3. Sll in Subspace II.

θ_0	φ_0	SLL (dB) $\sqrt{u^2+v^2} \le 0.2$	SLL (dB) $\sqrt{u^2+v^2} > 0.2$
20°	0°	-31.1	-14.2
20°	55°	-40.7	-13.3
20°	-55°	-38.5	-13.3
34.9°	0°	-30.1	-13
34.9°	55°	-37.8	-13
34.9°	-55°	-37.4	-13

Subspace II

The weighting phases are depicted in Fig. 9. The gain loss is 1.72 dB and the power is not attenuated, therefore, the taper loss is 1.72 dB, less than the required 2 dB.

The SLL values in the two regions, $0 \le \sqrt{u^2+v^2} \le 0.2$ and $0.2 < \sqrt{u^2+v^2} \le 1$ are summarized in TABLE 3 when the main beam scans at representative directions. The results meet all SLL requirements.

Similarly, the radiation patterns with main beam scans at $\theta_0 = 35°$, $\varphi_0 = 0°$ and $\theta_0 = 35°$, $\varphi_0 = 55°$ are given in Fig. 10 and Fig. 11, respectively.

Subspace III

The synthesized weighting phases are depicted in Fig. 12. The gain loss is only 0.51 dB and the power is not attenuated, hence the taper loss is 0.51 dB, far less than the required 2dB.

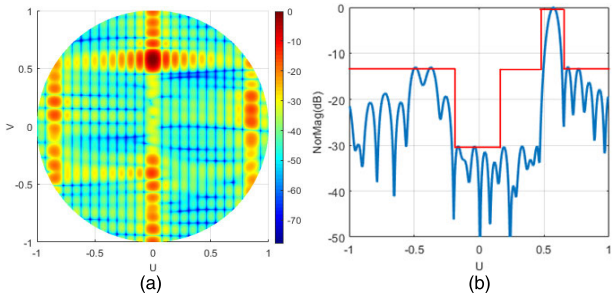

FIGURE 10. Patterns with main beam scans at ($\theta_0 = 34.9°$, $\varphi_0 = 0°$). (a) 3-D pattern, (b) *u*-cuts.

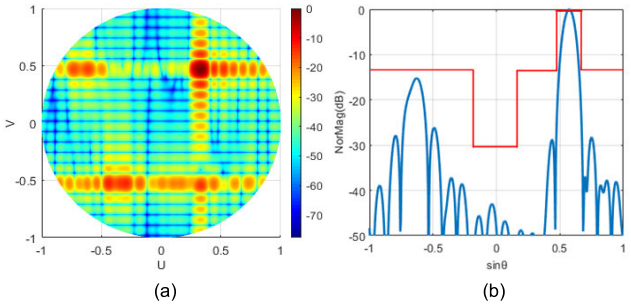

FIGURE 11. Patterns with main beam scans at ($\theta_0 = 34.9°$, $\varphi_0 = 55°$). (a) 3-D pattern, (b) 2D pattern with $\varphi = 55°$.

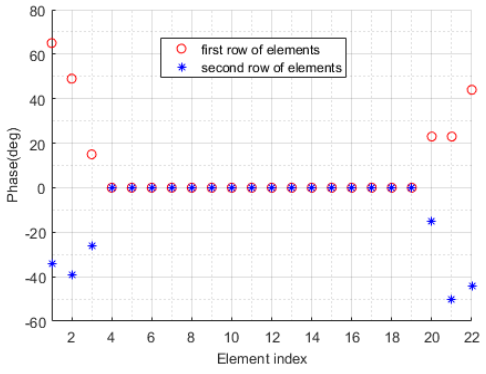

FIGURE 12. Weighting phases.

TABLE 4. Sll in Subspace III.

θ_0	φ_0	SLL (dB) $\sqrt{u^2+v^2} \le 0.2$	SLL (dB) $\sqrt{u^2+v^2} > 0.2$
35°	0°	-40.3	-13.8
35°	55°	-38.6	-13.5
35°	-55°	-35.4	-13.5
60°	0°	-38.1	-13.6
60°	55°	-34.3	-13.2
60	-55°	-33.3	-13.2

The SLL values in the two corresponding regions are summarized in TABLE 4 when the main beam scans at representative directions. The SLL meets all requirements.

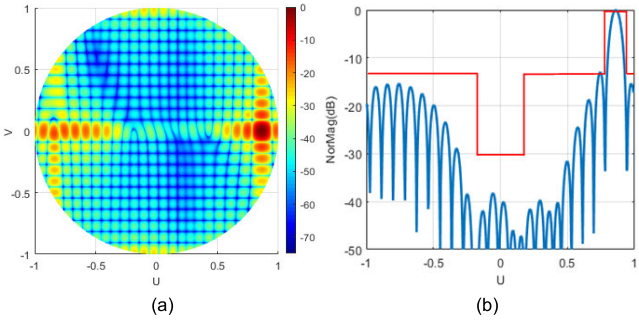

FIGURE 13. Patterns with main beam scanning at ($\theta_0 = 60°$, $\varphi_0 = 0°$). (a) 3-D pattern, (b) *u*-cuts.

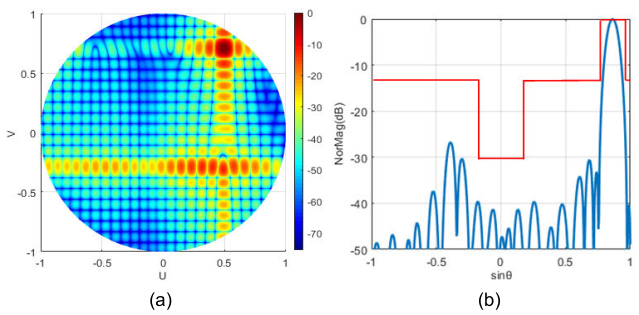

FIGURE 14. Patterns with main beam scanning at ($\theta_0 = 60°$, $\varphi_0 = 55°$). (a) 3-D pattern, (b) 2D pattern with $\varphi = 55°$.

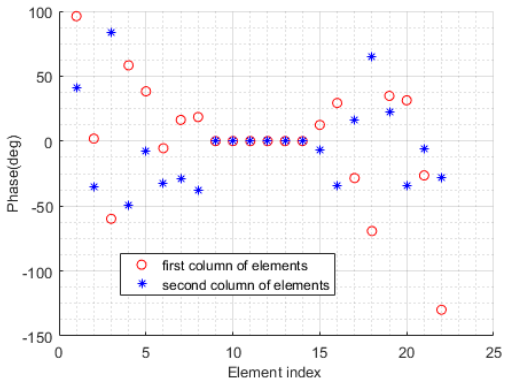

FIGURE 15. Weighting phases.

The radiation patterns with main beam scans at θ_0 =60°, φ_0 =0° and θ_0 =60°, φ_0 =55° are given in Fig. 13 and Fig. 14, respectively.

Subspace IV

The weighting phases are depicted in Fig. 15. The gain loss is 1.69 dB and the power is not attenuated, therefore, the taper loss is also 1.69 dB, less than the required 2 dB.

The SLL values in the two regions, $0 \le \sqrt{u^2+v^2} \le 0.2$ and $0.2 < \sqrt{u^2+v^2} \le 1$, are summarized in TABLE 5 when the main beam scans at representative directions. Therefore, the synthesized SLL also meets all requirements.

The radiation patterns with main beam scans at $\theta_0 = 34.9°$, $\varphi_0 = 90°$ and $\theta_0 = 34.9°$, $\varphi_0 = 125°$ are given in Fig. 16 and Fig. 17, respectively.

TABLE 5. Sll in Subspace IV.

θ_0	φ_0	SLL (dB) $\sqrt{u^2+v^2} \le 0.2$	SLL (dB) $\sqrt{u^2+v^2} > 0.2$
20°	90°	-31.1	-13.4
20°	55°	-31.6	-13.3
20°	125°	-31.4	-13.3
34.9°	90°	-30.3	-14.6
34.9°	55°	-32.6	-13.4
34.9°	125°	-33.3	-13.4

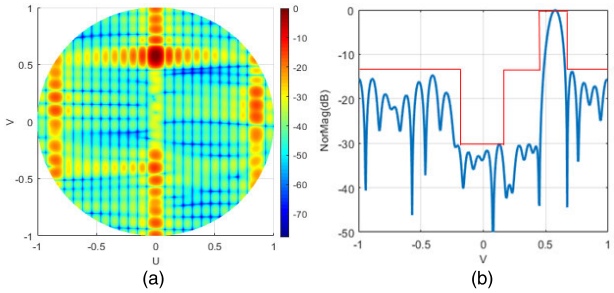

FIGURE 16. Patterns with main beam scanning at ($\theta_0 = 34.9°$, $\varphi_0 = 90°$). (a) 3-D pattern, (b) v-cuts.

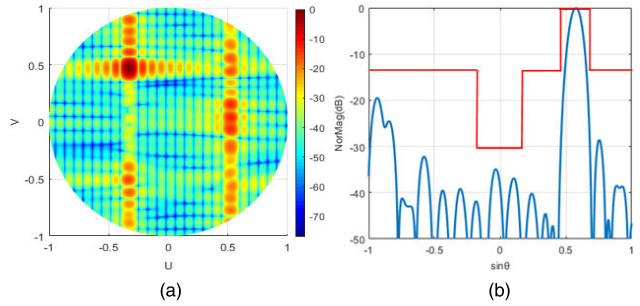

FIGURE 17. Patterns with main beam scanning at ($\theta_0 = 34.9°$, $\varphi_0 = 125°$). (a) 3-D pattern, (b) 2D pattern with $\varphi = 125°$.

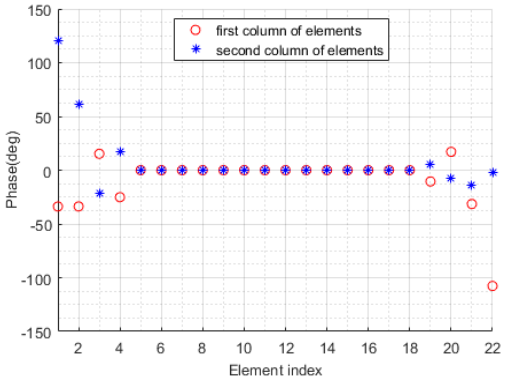

FIGURE 18. Weighting phases.

Subspace V

The weighting phases are depicted in Fig. 18. The gain loss is only 0.88 dB and the power is also not attenuated, thus the taper loss is 0.88dB, far less than the required 2dB.

TABLE 6. Peak Sll and Taper Loss in Subspace V.

θ_0	φ_0	SLL (dB) $\sqrt{u^2+v^2} \le 0.2$	SLL (dB) $\sqrt{u^2+v^2} > 0.2$
35°	90°	-32.5	-13.9
35°	55°	-39.1	-13.2
35°	125°	-36	-13.2
49.9°	90°	-32.1	-13.4
49.9°	55°	-35.6	-13.8
49.9°	125°	-34.2	-13.9

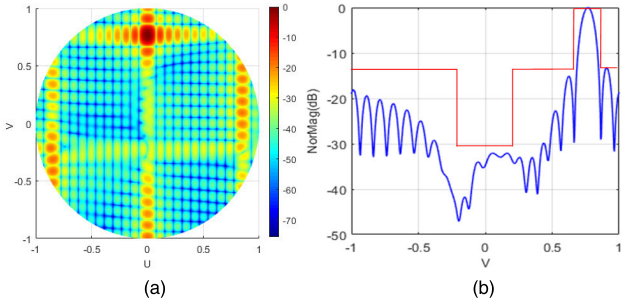

FIGURE 19. Patterns with main beam scanning at ($\theta_0 = 50°$, $\varphi_0 = 90°$). (a) 3-D pattern, (b) v-cuts.

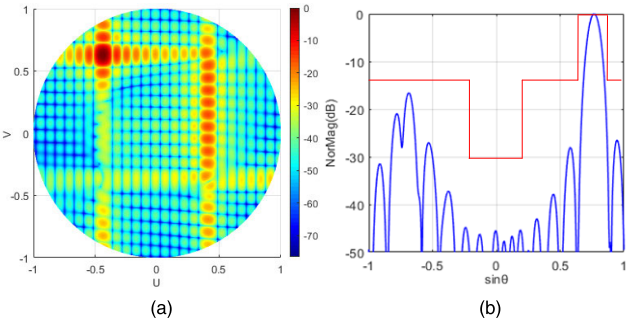

FIGURE 20. Patterns with main beam scanning at ($\theta_0 = 50°$, $\varphi_0 = 125°$). (a) 3-D pattern, (b) 2D pattern with $\varphi = 125°$.

The SLL values in the two regions, $0 \le \sqrt{u^2+v^2} \le 0.2$ and $0.2 < \sqrt{u^2+v^2} \le 1$ are summarized in TABLE 6 when the main beam scans at representative directions. Obviously, PSLL meets the requirements.

The radiation patterns with main beam scans at $\theta_0 = 34.9°$, $\varphi_0 = 90°$ and $\theta_0 = 34.9°$, $\varphi_0 = 125°$ are given in Fig. 19 and Fig. 20, respectively.

Subspace VI

The weighting phases are depicted in Fig. 21. The gain loss is only 1.11 dB and the power is also not attenuated, thus the taper loss is also 1.11 dB, far less than 2 dB.

The SLL values in the two corresponding regions are summarized in TABLE 7 when the main beam scans at representative directions. The synthesized SLL meets all requirements.

The radiation patterns with main beam scans at $\theta_0 = 60°$, $\varphi_0 = 90°$ and $\theta_0 = 60°$, $\varphi_0 = 125°$ are respectively given in Fig. 21 and Fig. 22 so that to have a more straightforward illustration of the SLL.

TABLE 7. SII and Taper Loss in Subspace VI.

θ_0	φ_0	SLL (dB) $\sqrt{u^2+v^2} \le 0.2$	SLL (dB) $\sqrt{u^2+v^2} > 0.2$
50°	0°	-32.3	-13.9
50°	0°	-33.4	-13.5
50°	45°	-36.7	-13.6
60°	90°	-31.4	-13.6
60°	55°	-30.2	-13.1
60°	125°	-34.5	-13.2

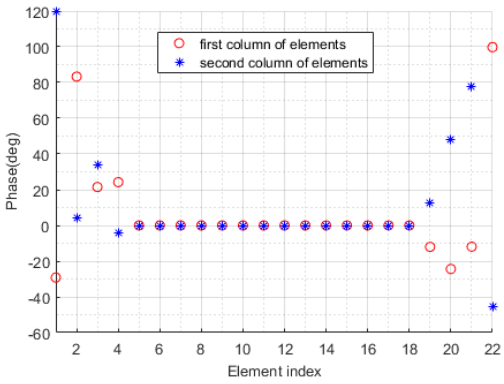

FIGURE 21. Weighting phases.

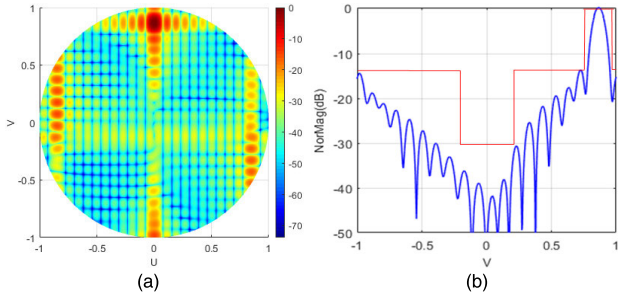

FIGURE 22. Patterns with main beam scanning at ($\theta_0 = 60°$, $\varphi_0 = 90°$). (a) 3-D pattern, (b) v-cuts.

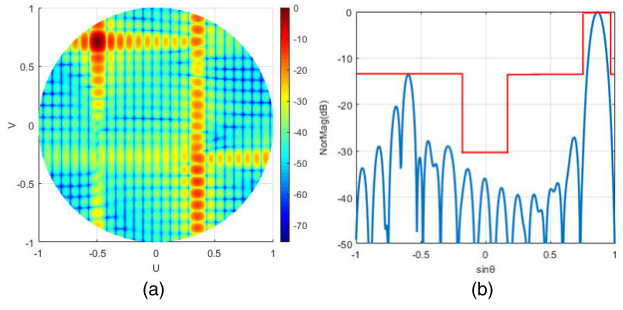

FIGURE 23. Patterns with main beam scanning at ($\theta_0 = 60°$, $\varphi_0 = 125°$). (a) 3-D pattern, (b) 2D pattern with $\varphi = 125°$.

In conclusion, all specific requirements from the practical application have been successfully met as summarized in TABLE 8.

TABLE 8. SII in Each Subspace.

subspace		SLL (dB) required	SLL (dB) achieved	taper loss(dB) required	taper loss(dB) achieved
I	$0 \le \sqrt{u^2+v^2} \le 1$	≤ -25	≤ -25.3	≤ 5.5	5.4
II	$\sqrt{u^2+v^2} \le 0.2$	≤ -30	≤ -30.1	≤ 2	1.72
	$\sqrt{u^2+v^2} > 0.2$	≤ -13	≤ -13		
III	$\sqrt{u^2+v^2} \le 0.2$	≤ -30	≤ -33.3	≤ 2	0.51
	$\sqrt{u^2+v^2} > 0.2$	≤ -13	≤ -13.2		
IV	$\sqrt{u^2+v^2} \le 0.2$	≤ -30	≤ -30.3	≤ 2	1.69
	$\sqrt{u^2+v^2} > 0.2$	≤ -13	≤ -13.2		
V	$\sqrt{u^2+v^2} \le 0.2$	≤ -30	≤ -32.1	≤ 2	0.88
	$\sqrt{u^2+v^2} > 0.2$	≤ -13	≤ -13.2		
VI	$\sqrt{u^2+v^2} \le 0.2$	≤ -30	≤ -30.2	≤ 2	1.11
	$\sqrt{u^2+v^2} > 0.2$	≤ -13	≤ -13.1		

VI. CONCLUSION

In recent years, APAA has been increasingly applied in satellites. In a practical satellite application, at some MBSA, extremely SLL in some local space is needed. The harsh limitation on APAA taper loss further complicates the problem seriously. It imposes tough challenge to antenna engineers. Classic synthesis methods applying a single set of weights regardless of the scanning angle fail to produce qualified APAA.

In this paper, a scanning space-division and array-decomposition approach is proposed to solve this hard problem. Different weights are implemented when the APAA is scanning at different angles. This transforms the nearly unsolvable problem into multiple solvable problems. In addition, to ease the synthesis problem in each subspace, the entire array is simplified as an assembly of multiple sub-arrays. Each and every sub-array shares the same set of scanning angle-dependent weights. The number of synthesis parameters is therefore reduced to the order of the subarray that the synthesis is much easier to solve without sacrificing too much synthesis performance.

Based on the proposed approach, SFFT has been applied to solve the amplitudes of the APAA corresponding to the subspace I, and DDE has been applied to optimize the phases of sub-array corresponding subspace II∼VI. All specific requirements including SLL and taper loss have been successfully met.

Although the practical application problem has been successfully solved, however, due to security and commercial restrictions, publishing measurement results is strictly prohibited.

REFERENCES

[1] G. Y. Zhang and Y. J. Zhao, *Phased Array Radar Technology*. Beijing, China: Publishing House of Electronic Industry, (in Chinese), 2006.
[2] E. Sharp, "A triangular arrangement of planar-array elements that reduces the number needed," *IRE Trans. Antennas Propag.*, vol. 9, no. 2, pp. 126–129, Jul. 1961.

[3] A. Safaai-Jazi, "A new formulation for the design of Chebyshev arrays," *IEEE Trans. Antennas Propag.*, vol. 42, no. 3, pp. 439–443, Mar. 1994.
[4] A. Safaai-Jazi, "Directivity of Chebyshev arrays with arbitrary element spacing," *Electron. Lett.*, vol. 31, no. 10, pp. 772–774, May 1995.
[5] J. M. Cid, J. A. Rodríguez, F. Ares, and E. Moreno, "Sythesis of satellite footprints by perturbation of woodward-lawson solutions for planar array antennas," *J. Electromagn. Waves Appl.*, vol. 14, no. 1, pp. 3–10, 2000.
[6] F. J. Ares-Pena, J. A. Rodriguez-Gonzalez, E. Villanueva-Lopez, and S. R. Rengarajan, "Genetic algorithms in the design and optimization of antenna array patterns," *IEEE Trans. Antennas Propag.*, vol. 47, no. 3, pp. 506–510, Mar. 1999.
[7] D. W. Boeringer, D. H. Werner, and D. W. Machuga, "A simultaneous parameter adaptation scheme for genetic algorithms With application to phased array synthesis," *IEEE Trans. Antennas Propag.*, vol. 53, no. 1, pp. 356–371, Jan. 2005.
[8] D. W. Boeringer and D. H. Werner, "Particle swarm optimization versus genetic algorithms for phased array synthesis," *IEEE Trans. Antennas Propag.*, vol. 52, no. 3, pp. 771–779, Mar. 2004.
[9] T. H. Ismail and Z. M. Hamici, "Array pattern synthesis using digital phase control by quantized particle swarm optimization," *IEEE Trans. Antennas Propag.*, vol. 58, no. 6, pp. 2142–2145, Jun. 2010.
[10] Y. Chen, S. Yang, and Z. Nie, "The application of a modified differential evolution strategy to some array pattern synthesis problems," *IEEE Trans. Antennas Propag.*, vol. 56, no. 7, pp. 1919–1927, Jul. 2008.
[11] C. Lin, A. Qing, and Q. Feng, "Synthesis of unequally spaced antenna arrays by using differential evolution," *IEEE Trans. Antennas Propag.*, vol. 58, no. 8, pp. 2553–2561, Aug. 2010.
[12] L. Shi, H.-F. Sun, R. Wang, J.-Q. Ai, H. Yan, and Y.-K. Deng, "An improved real-coded genetic algorithm for the beam forming of spaceborne SAR," *IEEE Trans. Antennas Propag.*, vol. 60, no. 6, pp. 3034–3040, Jun. 2012.
[13] W. P. M. N. Keizer, "Fast low-sidelobe synthesis for large planar array antennas utilizing successive fast Fourier transforms of the array factor," *IEEE Trans. Antennas Propag.*, vol. 55, no. 3, pp. 715–722, Mar. 2007.
[14] R. J. Mailloux, *Phased Array Antenna Handbook*, 2nd ed. Boston, MA, USA: Artech House, 2005.
[15] R. S. Elliott, *Antenna Theory and Design*. Hoboken, NJ, USA: Wiley, 2003.
[16] A. Qing, "Dynamic differential evolution strategy and applications in electromagnetic inverse scattering problem," *IEEE Trans. Geosci. Remote Sens.*, vol. 44, no. 1, pp. 116–125, Jan. 2006.